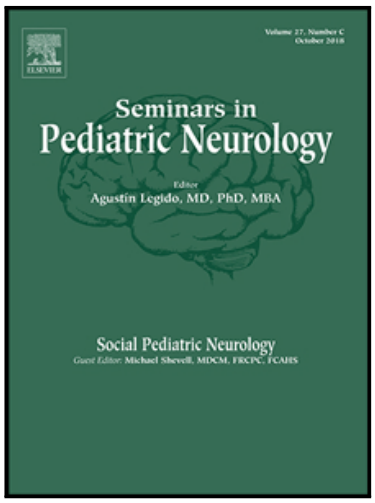

A Comprehensive Framework for Differentiating Autism Spectrum Disorder from Neurotypicals by Fusing Structural MRI and Resting State Functional MRI

Omar Dekhil , Mohamed Ali , Reem Haweel , Yaser Elnakib , Mohammed Ghazal , Hassan Hajjdiab , Luay Fraiwan , Ahmed Shalaby , Ahmed Soliman , Ali Mahmoud , Robert Keynton , Manuel F. Casanova , Gregory Barnes , Ayman El-Baz

PII: S1071-9091(20)30011-5
DOI: https://doi.org/10.1016/j.spen.2020.100805
Reference: YSPEN 100805

To appear in: *Seminars in Pediatric Neurology*

Please cite this article as: Omar Dekhil , Mohamed Ali , Reem Haweel , Yaser Elnakib , Mohammed Ghazal , Hassan Hajjdiab , Luay Fraiwan , Ahmed Shalaby , Ahmed Soliman , Ali Mahmoud , Robert Keynton , Manuel F. Casanova , Gregory Barnes , Ayman El-Baz , A Comprehensive Framework for Differentiating Autism Spectrum Disorder from Neurotypicals by Fusing Structural MRI and Resting State Functional MRI, *Seminars in Pediatric Neurology* (2020), doi: https://doi.org/10.1016/j.spen.2020.100805

A Comprehensive Framework for Differentiating Autism Spectrum Disorder from Neurotypicals by Fusing Structural MRI and Resting State Functional MRI

Omar Dekhil[*,a], Mohamed Ali[*,a], Reem Haweel[*], Yaser Elnakib[*], Mohammed Ghazal[†], Hassan Hajjdiab[†], Luay Fraiwan[†], Ahmed Shalaby[*], Ahmed Soliman[*], Ali Mahmoud[*], Robert Keynton[*], Manuel F. Casanova[‡], Gregory Barnes[§], and Ayman El-Baz[*]

From the [*]Department of Bioengineering, University of Louisville, Louisville, KY, USA.
[†]Department of Electrical and Computer Engineering, Abu Dhabi University, Abu Dhabi, United Arab Emirates.
[‡]Department of Biomedical Sciences, University of South Carolina, Greenville, SC, USA.
[§]Department of Neurology, University of Louisville, Louisville, KY, USA.

This work was supported in part by the University of Louisville 21st Century University Initiative on Big Data in Medicine.

Address reprint requests to Ayman El-Baz, Deparment of Bioengineering, Lutz Hall Suite 419, Louisville, KY 40292. E-mail: ayman.elbaz@louisville.edu

[a] These authors contributed equally to the manuscript.

Abstract

Autism spectrum disorder is a neuro-developmental disorder characterized by impaired social abilities and communication difficulties. The golden standard for autism diagnosis in research rely on behavioral features, e.g., the autism diagnosis observation schedule (ADOS), the Autism Diagnostic Interview-Revised (ADI-R). In this study we introduce a computer-aided diagnosis (CAD) system that uses features from structural MRI (sMRI) and resting state functional MRI (fMRI) to help predict an autism diagnosis by clinicans. The proposed system is capable of parcellating brain regions to show which areas are most likely affected by autism related abnormalities and thus help in targeting potential therapeutic interventions. When tested on 18 data sets (n = 1060) from the ABIDE consortium, our system was able to achieve high accuracy (sMRI 0.75-1.00; fMRI 0.79-1.00), sensitivity (sMRI 0.73-1.00; fMRI 0.78- 1.00), and specificity (sMRI 0.78-1.00; fMRI 0.79-1.00). The proposed system could be considered an important step towards helping physicians interpret results of neuroimaging studies and personalize treatment options. To the best of our knowledge, this work is the first to combine features from structural and functional MRI, use them for personalized diagnosis and achieve high accuracies on a relatively large population.

Introduction

Autism spectrum disorder (ASD) is a neuro-developmental disorder characterized by social and behavioral impairments.[1] Previous work has reported a correlation between the severity of autism and both functional activation and anatomical abnormalities.[2] Structural MRI (sMRI) is the most commonly used imaging modality for screening anatomical anomalies in both research and clinical practice.[3] By way of contrast, changes in blood flow, putatively related to neuronal activation, is assessed using functional MRI (fMRI).[4]

When studying structural MRIs, two main elements lend themselves to analysis: (i) shape, and (ii) volumetric features. Structural MRI study uses features derived from one or both. A study conducted on 60 autistic and 52 typically developed (TD) subjects analyzed anatomical anomalies in cerebral and cerebellar volumes of autistic brains.[5] 50% of autistic participants in that study were in the age of 5 years or older (group one) and the rest were in the age range of 2 to 4 years (group two). 90% of participants within group two showed brain volumes larger than normal. The result was supported by a subsequent study,[5] using the same patient population, that found an increase in the cerebellar white matter volume in autistic subjects (group 2) as compared to controls. Other studies have emphasized that the cerebral hemispheres can remain enlarged during adulthood.[6] It was suggested that the main areas of brain enlargement appear to be the frontal, temporal, and parietal lobes.[7,8,9]

More insightful results were achieved when considering changes in cortical volume (CV) to be the result of the product of 2 independent parameters: cortical thickness (CT) and surface area (SA).[10] The study analyzed three parameters (CV, CT, and SA) and found a significant increase in the CT of ASD subjects as compared to TD individuals in the frontal lobe regions. By contrast, the SA in the orbitofrontal cortex and posterior cingulum in the autistic subjects was reduced as compared to the control group. Further study based on those 3 parameters reported similar results.[11] The study of longitudinal changes in cortical thickness allows the identification of specific regional differences in the CT. One such study, discovered that the most significant differences in CT between ASD and TD individuals of the same mean age were in the bilateral inferior frontal gyrus, pars opercularis, pars triangularis, right caudal middle frontal, and left rostral middle frontal regions.[12] However, significant differences in other brain regions have also been reported. For instance, autistic subjects have displayed a larger amygdala than TD subjects.[13] In examining the areas believed to be responsible for the social cognitive functions: in particular, (1) facial recognition (right fusiform gyrus), (2) perception and eye gaze (superior temporal gyrus), and (3) mental state attribution (anterior cingulate and superior temporal sulcus), a significant increase in the grey matter volume was observed in these brain regions.[14] Another study examining the cerebellum, fusiform gyrus, and frontal cortex[15] found increased grey matter volume in the cerebellum.

One of the main technological advancements introduced to differentiate between the neurotypical and autistic brains is shape-based analysis. One widely studied morphometric parameter has been the gyrification index (GI), which has been used as a quantitative measure of cortical folding for shape analysis.[16,17] Calculated from MRI slices, GI is the ratio between total contour length and outer contour length of a gyrus. It was reported that the GI in the left frontal area is larger in ASD adolescents and children compared to TD peers[17]. It has also been noted that the GI decreases with age in ASD individuals while it does not in TD

subjects. An additional supporting result for increased GI in ASD individuals was a reported increased gyrification in the bilateral posterior cortices.[18] In addition, it has been noted that typically developing individuals showed a positive correlation between gyrification and vocabulary knowledge in the left inferior parietal cortex while no similar correlation was found in autistic individuals. An additional example of folding analysis introduced 6 folding measures used to discriminate between ASD and TD groups.[19] These 6 folding measures were: (i) Shape index, (ii) Curvedness, (iii) Isoperimetric ratio, (iv) Convexity ratio, (v) Intrinsic curvature index, and (vi) Mean curvature norm. Increased folding was noted in the temporal, frontal and parietal lobes of ASD individuals as compared to TD controls. This increased folding was more prominent in children than adults. A more recent study extracted seven features from a reconstructed brain mesh to address the curvature abnormalities.[20] The examined features included: (i) mean curvature, (ii) thickness, (iii) Gaussian curvature, (iv) folding index (v) standard deviation, (vi) volume, and (vii) surface area. The study noted that diagnostic accuracy could be increased when clinical features were added to their classification algorithm. Another study used surface-based morphometry to examine the cortical shape abnormalities in low and high functioning ASD individuals.[21] To analyze such abnormalities, sulcal depth was used as a quantitative measure. In both low-functioning and high-functioning ASD individuals, similar abnormalities in sulcal depth were observed mainly in the frontal operculum and anterior insula, with slightly smaller size noted in high-functioning ASD subjects. Also, the inferior frontal gyrus had shape abnormalities that were centered near the ventral postcentral gyrus and parietal operculum. Sulcal depth differences were also reported for the anterior-insula and temporoparietal junction in both ASD and TD groups.[22] Temporal and frontal areas exhibited the most significant abnormalities, specifically for the social and language regions in autistic groups, which were severely affected. An investigation of brain shape differences using the GI index reported a prominent increase in gyrification around the post-central and left pre-gyrus in ASD individuals.[23]

To study the brain functional activation anomalies, analysis of the fMRI modality is performed by applying two major types of experiments, (i) resting state fMRI (RfMRI) and (ii) task-based fMRI.[24] The underconnectivity theory was first introduced as a way of explaining both the neurobiological and cognitive abnormalities observed in ASD.[25] Reduced synchronized brain activity is a main hallmark for cognitive disorders.

Task-based approaches are studied to identify brain areas activated in response to certain tasks. An example of such tasks was a visual figures experiment,[26] which identified lower activation in the inferior parietal and the left dorsolateral prefrontal areas, and higher activation bilaterally in the superior parietal and the right occipital (visuospatial) areas of ASD subjects. Another example is the response to facial expressions,[27] where higher activation in the ventral prefrontal cortex, striatum, and amygdala was reported for autistic subjects.

Another paradigm studied is the rewards task, in which the brain activity is monitored in response to rewards, e.g., social reward or monetary rewards.[28,29] ASD individuals were reported to have more activation in the anterior cingulate gyrus and left mid-frontal gyrus and less activation in the right nucleus accumbens during the response to social and monetary rewards.[30]

Studies of resting state fMRI investigate alterations in brain connectivity between TD and ASD groups.[31] In a recent study, a machine learning algorithm based on a multivariate

autoregressive model was used to study functional connectivity.[32] The study found that ASD subjects had reduced functional connectivity; results which also lend credence to the theory of underconnectivity in autism. Similarly, reduced functional connectivity in the superior parietal and visuospatial areas was reported in ASD as compared to TD.[33] Another study showed reduced connectivity in both the temporal and frontal cortex, while no global abnormalities were detected.[34] Abnormalities in the functional networks were reported as being more evident in social information processing related networks.[35]

ASD have not only shown results that indicate brain underconnectivity, as in the previous studies, but also increased connectivity for some areas compared to healthy control subjects.[36] The research studied alternations of functional connectivity patterns, specifically the interhemispheric connectivity analysis, and showed both decreased and increased connectivity in ASD subjects. Another supporting study reported hyperconnectivity in autistic children with more severe social dysfunction.[37] The presence of altered connectivity was also confirmed.[38] Both hypoconnectivity and hyperconnectivity were present in ASD subjects.

In addition to reporting global differences between ASD and TD groups, resting state connectivity patterns demonstrated promising results in diagnosing many diseases e.g., Alzheimer's disease and schizophrenia.[39,40] A recent study used functional connectivity analysis with the deep neural network to diagnose autism.[41] It fed the classification network input with the functional connectivity correlation matrix. This experiment achieved an accuracy of 70%.

The marked clinical heterogeneity noted in autism suggests the importance of considering both the anatomical and physiological characteristics of individual subjects when entertaining a possible diagnosis. We believe that combining both sMRI and fMRI will bear results that correlate more closely with the autistic behavior, thus improving diagnostic sensitivity, accuracy and specificity. In the proposed system, functional and anatomical features are used by a machine-learning algorithm to help clinicians establish a personalized autism diagnosis.

Material and Methods

In this study, the data for both structural and functional MRI was obtained from ABIDE I dataset (http://fcon_1000.projects.nitrc.org/indi/abide/abide_I.html). The ABIDE I was collected from 18 different sites with total number of subjects $n = 1060$ (561 autistic and 521 typically developed). The demographics of the subjects are provided in their respective tables. Demographic data includes the age, gender, full scale IQ, performance IQ, verbal IQ and hand dominance for each group. The scanning parameters of both structural and functional MRI are given. These parameters include scanner type, scanning protocol, repetition time (TR), echo time (TE), flipping angle and experiment duration for fMRI. All of the information is publicly available in the ABDIE dataset website. Figure 1 illustrates the whole pipeline of the proposed methodology in this study.

Structural MRI experiment

The sMRI study was divided into 2 main parts: (i) data preprocessing, brain segmentation and cortex reconstruction and (ii) extraction of both volumetric and morphological features. The pre-processing steps could be summarized as follows:

Preprocessing, brain segmentation and cortex reconstruction

1. Intensity normalization:[42] In this step, a non-parametric model is used to correct intensity non-uniformities. This model does not require any prior information about tissues classification in the image. This step is important in order to overcome the variability of scanners effect.
2. Skull stripping:[43] In this step, brain extraction tool (BET) algorithm is used. This algorithm combines both watershed algorithm and deformable surface model[43].

Brain segmentation and area labeling

In this step, a combined model, that uses both shape and intensity models, is used to segment brain tissues into gray matter, white matter and CSF.[44,45]

Having the preprocessing and segmentation completed, a second set of steps is applied for cortex reconstruction and anatomical atlas parcellation to an anatomical template.

1. Defining the gray-white matter boundary:[46,47] In this step, the gray-white matter surface is accurately detected by correcting the topological defects by iterative opening and sealing algorithm.
2. Surface inflation and spherical atlas registration:[48,49] In this step, a 3D sphere is constructed and the cortical surface is inflated on this sphere. The surface is then parameterized to fit on the sphere to create a spherical based coordinate system.
3. Cortical surface parcellation to the Desikan-Killiany (DK) atlas:[50] In this step, the brain is parcellated to 68 areas (34 areas per hemisphere)

After completing the above steps, 8 features are calculated for each of the 34 hemisphere areas. The 8 calculated features for each DK atlas area are displayed in Table 1.

In this study, the FreeSurfer pipeline was used for all of the preprocessing and feature extraction steps mentioned above. FreeSurfer is a widely used tool for MRI analysis and it is freely available for download (http://surfer.nmr.mgh.harvard.edu/).

Since the data are collected from multiple sites and with different criteria, possible variability may be accounted by some confounding variables. For example, age mismatch or IQ differences may affect the calculated features values. To address such problem, a per-subject normalization algorithm was utilized. This algorithm uses the differences between a couple of areas (Delta matrix) instead of using the value from each area. In this way, the individual abnormalities are better addressed. By building this delta matrix the feature value per area is compared to the other values within the subject, then this difference is used for intra-subject variability. For each feature, a 68×68 matrix is constructed. This leads to feature matrix of size 68x68x8 per subject. The pipeline of sMRI experiment is shown in Figure 2.

Functional MRI experiment

In order to examine the functional connectivity between different brain areas, the correlation between the activation courses is then used as a measure of functional connectivity. The data used in this experiment are the preprocessed data provided by the ABIDE dataset. The selected preprocessing pipeline is the Connectome Computation System (CCS) pipeline, where the first 4 volumes are dropped; slice timing correction, motion correction, and intensity normalization are performed. To overcome the subject's motion-related confounding variables, 24 motion parameters are used as regressors. To remove their effect, the mean white matter and CSF are also regressed out. Finally, the fMRI volumes are registered to MNI-152 standard space. The registration consists of 2 stages. First, each fMRI volume is registered to the corresponding structural T1-weighted volume, and then the structural volume is registered to the standard space image.

In order to study the coherence between different brain areas, the functional connectivity was selected to be the feature of interest in this study. The reason behind this selection is its ability to identify the intrinsic functional network in the brain. As mentioned in the introduction, the alternations in connectivity within and between the networks has been reported to be of use for diagnosing autism.[51]

Since we are using in this study the AAL cortical parcellation, the functional connectivity matrix is constructed between each pair of its 116 areas. The Pearson correlation coefficient (ρ) is used to calculate the functional connectivity between each pair of areas in the atlas. Figure 3 shows how to construct the connectivity feature matrix.

Local and global analysis

In this study, the same classification pipeline is applied to both sMRI and fMRI. As mentioned above, the fMRI features are a 116x116 connectivity matrix, F per subject.

$$F = \begin{bmatrix} \rho_{1,1} & \rho_{1,2} & \cdots \\ \vdots & \ddots & \\ \rho_{n,1} & & \rho_{116,116} \end{bmatrix} \quad (1)$$

Where $\rho_{i,j}$ is the correlation coefficient between the activation time courses in i^{th} and j^{th} areas and n is the index of areas ($n = 116$). The constructed feature matrix for sMRI features S is a $68 \times 68 \times 8$ matrix per subject, where each element is the difference between the feature value at i^{th} and j^{th} areas.

$$S_f = \begin{bmatrix} \Delta_{1,1,f} & \Delta_{1,2,f} & \cdots \\ \vdots & \ddots & \\ \Delta_{68,1,f} & & \Delta_{68,68,f} \end{bmatrix} \quad (2)$$

Where S_f is the feature matrix of the feature f and $S_{i,j,f}$ is the difference in the values of feature f between areas i and j.

For each of the elements in both feature matrices, this element is fed to a local classifier first. Both the accuracy and the output probability of each feature belonging to an autism class are calculated from the local classifiers. The selected local classifiers in this study is K-nearest neighbors (KNN) classifiers with number of k = 7. After finishing the local classification phase, the features for each modality are sorted with respect to the local classification accuracy

achieved in the local classification step.

After completing the local analysis, the second step is to use the sorted list of feature vectors of both sMRI and fMRI for the per-modality analysis. In this step an incremental approach is used, where a single feature from the sorted list is added at time to the used feature vector. After adding each feature, we run our cross validation for the whole system and the accuracy is recorded. In this step a random forest classifier is used. To adjust the hyperparameters of the random forest (number of estimators and maximum depth of the tree) a grid search is used. The optimal cutoff is obtained by trying the top 100 features in the sorted feature list until reaching the maximum cross validation accuracy.

After finding the optimal cutoff threshold per modality, both sMRI and fMRI feature vectors are concatenated together and fed to another random forest classifier for the global analysis decision. The 2 steps classification approach used is illustrated in Figure 4.

RESULTS

Subjects demographics and cohort summary statistics

Table 2 shows the demographic summary statistics for each site for both the autistic and typically developing subjects. For each site, the number of males and females, age, verbal IQ, full IQ and performance IQ statistics are included. The listed statistics are the minimum, maximum, mean and standard deviation for both autistic and neurotypical subjects. Per-site distribution of people on the spectrum was significantly different across sites ($\chi^2 = 251,14\ df, p < 10^{-6}$). Six sites provided research-reliable ADOS calibrated severity scores. There was a trend towards significant differences in mean severity among these six sites ($F = 2.24, df = 5.224, p = 0.052$). Four sites administered the Social Responsiveness Scale. Among these sites, differences between the autism and control groups varied ($F = 2.95, df = 3{,}357, p = 0.0327$). Two sites (LEUVEN and SBL) administered the Social Communication Questionnaire, and two (LEUVEN and SBL) administered the Autism-Spectrum Quotient. Differences between ASD and control groups were consistent between sites (interaction effect p = 0.550 and 0.996, respectively). Differences in full-scale IQ and verbal IQ between ASD and control varied significantly per site ($F = 2.18, df = 15{,}1007, p = 0.0058\ and\ F = 2.55, df = 11{,}892, p = 0.0035$, respectively). Differences in performance IQ did not, however (p = 0.34).

Local and global diagnosis

For each element in both structural and functional MRI feature matrices, the probability of this element belonging to the autism class is calculated. The output local probabilities form 2 matrices P_S and P_F with the same size as the feature matrices F and S.

$$P_F = \begin{bmatrix} pf_{1,1} & pf1{,}2 & \dots \\ \vdots & \ddots & \\ pf & & pf116{,}116 \end{bmatrix} \quad (3)$$

$$P_S f = \begin{bmatrix} Ps_{1,1,f} & Ps_{1,2,f} & \cdots \\ \vdots & \ddots & \\ Ps_{68,1,f} & & Ps_{68,68,f} \end{bmatrix} \quad (4)$$

where pf_{ij} and $Ps_{i,j,f}$ represent the probability of an element in the feature matrix of functional and structural feature matrices respectively to belong to the autism class.

To obtain the personalized maps, 2 vectors, V_f and V_s are calculated for fMRI and sMRI respectively.

$$V_f(i) = \max_{0 \le j \le 116} P_F(i,j) \quad (5)$$

$$V_s(i) = \max_{1 \le j \le 68, 1 \le f \le 8} P_S(i,j,f) \quad (6)$$

These 2 vectors entries holds the highest calculated probability of a feature to be belonging to the autism class. A sample of these color-coded maps is shown in Figure 5.

Per modality diagnosis results

After calculating the local probabilities from the first step, P_S and P_F, they are then sorted according to their local accuracy. A linear search is then performed to get the optimal length of the concatenated feature vector for sMRI and fMRI. Tables 3 and 4 shows the accuracy, sensitivity and specificity obtained from each site and the optimal length of the feature vector for this site.

The best results for sMRI were obtained with data derived from the "CMU", "OHSU", and "SBL" sites, where all subjects were correctly diagnosed. The lowest accuracy was derived from the "NYU" site. For the fMRI, the "OLIN" site achieved the best results, with all subjects correctly classified. The lowest accuracy was again derived from the "NYU" site. In order to achieve the highest accuracy, the maximum number of concatenated features was 75 for sMRI and 99 for fMRI.

Discussion

Autism is a disorder whose diagnosis is based on behavioral findings. Ever since its inception as a clinical entity, its recognition was contingent on the clinical skills of the interviewer and the subjective interpretation of his/her findings. This perspective was a throwback to the influence exerted by Adolf Meyer on his protégé Leo Kanner.[52] Meyer's conception of psychobiology depended on collecting detailed case histories that considered the social, environmental and medical factors that facilitated abnormal behaviors. Following the psychobiological precepts, Kanner reported copious clinical histories on eleven young children (eight boys and three girls, all younger than 11 years) initially diagnosed with childhood schizophrenia but who also exhibited an autistic withdrawal.[53] Kanner went on to describe precedents for similar children within the medical literature. Based primarily on his clinical acumen, and further patient documentation, he advocated for autism as a sui generis developmental disorder. The mode of diagnosis thus pursued by Kanner and his followers

necessitated the instantiation of behaviors that sometimes were age dependent. This incurred in a delay for both obtaining a diagnosing and therapeutic implementation until such behaviors were abundantly clear. Furthermore, without any pathognomonic symptoms, behaviors lent themselves to multiple interpretations creating a diagnostic spectrum that included atypical presentations. The inherent lack of clinical homogeneity in any given subject sample has clouded research efforts for most of the recorded history of autism. The last decade has brought advancements in both anatomical and physiological assessment techniques, which allow us to combine insights from clinical observations with laboratory test results.

In this study, an algorithm combining evidence from both structural and functional MRI revealed an accuracy, sensitivity, and specificity in differentiating autism from neurotypicals that ranged from 0.7 to 1. One weakness of the study is that no other neurodevelopmental condition was tested. It is thus possible that the specificity of the algorithm would diminish when adding other groups that are on the differential diagnosis of autism, e.g., ADHD, spatial ataxia, speech delay. Although not diagnostic, the results suggest the improved predictability of an autism diagnosis while still pending behavioral manifestations of the disorder. This may be of special use in evaluating at risk children, e.g., infants with an older diagnosed sibling, cases of extreme prematuriy, intrauterine viral infections. It is generally accepted that early detection and therapeutic intervention in these cases may lead to better outcomes.[54] Previous studies in the literature[20] suggest that adding elements of the clinical history to our algorithm may improve the accuracy of the results; a line of inquiry that we are presently pursuing. Furthermore, the ability of the algorithm to provide regionalized assessments according to brain parcellation gives the added advantage of guiding potential therapeutic interventions by targeting affected sites. A patient whose primary abnormalities arise from the prefrontal lobes may gain from therapies, reward systems, and classroom accommodations built to strengthen executive skills. Alternatively, a patient whose primary abnormalities arise from the language regions of the brain may similarly gain from speech therapy. This interesting line of inquiry, as to differing potential interventions based on gross anatomical findings, to our knowledge, has not been previously pursued in the autism literature.

This study extends our previous fMRI work,[29,55,56] to suggest that some anatomical MRI parameters related to brain anatomy and morphology including curvature, surface area, and volume are relevant to defining ASD related circuitry abnormalities.[57] In essence, the aforementioned parameters stand as anthropometric indices of brain connectivity.[58] Neocorticalization in primates has progressed through the expansion of axonal mass, rather than an increase in the total number of cortical neurons.[59] Changes in the size and shape of the cerebral cortex have concurrently given rise to the altered arrangement of white matter fibers, and alterations in the gray/white matter.[58]

It is generally accepted that the results of a study depend on the quality of the data collected. Data from our study was obtained from an international depository created by numerous brain imaging laboratories. Each contributing partner made the decision as to how best collect data based on their ongoing research interests. Inclusionary and exclusionary criteria for participation varied across imaging sites. Differences in diagnostic criteria, age of participants, comorbidities and concomitant use of medical and alternative treatments could account for added variability and shifting of the statistical distribution away from mean values. Indeed, although all of the centers reporting data in the present study used DSM-IV-TR (De

Bildt)diagnostic criteria, the subject population fell along different points of the clinical spectrum. A per site distribution of autistic subjects (autism vs. Asperger vs. PDD-NOS) in our study showed significant differences (χ^2=251, 14 d.f., $p < 10^{-6}$). We approached this problem by implementing a per subject normalization algorithm that used the difference between areas (Delta matrix) as opposed to singular regional values. The procedural pipeline implementing this normalization is depicted in Figure 2.

The purpose of this study wasn't to perform a metaanalysis. The lack of standardized eligibility criteria would have prevented the analysis of data from the different sites selected. However, this same variability, both among subjects and MRI protocols, defines the type of imaging study brought to the attention of a clinician in his daily practice. The fact that our algorithm was able to attain a high degree of accuracy in the midst of this variability provides an attestation as to its potential clinical value. In effect, the diagnostic effect of our algorithm was consistent across different sites, thus adding power to the potential conclusion drawn from a single study. Despite the high dimensional feature space inherent in our study, the algorithm reported in this study successfully captured discriminating features across the entire dataset.

To the best of our knowledge, this is the first study to include all ABIDE dataset sites, and perform local analysis on the connectivity features extracted from each individual pair of areas in order to complete a whole brain connectivity analysis. This analysis can be used to provide a personalized map per subject to show affected brain areas and to gage the probability of a diagnostic difference when comparing autistic individuals to controls.

References

1. Frith U, Happé F: Autism spectrum disorder. Current Biology 15: R786–R790; 2005.
2. Aghdam MA, Sharifi A, Pedram MM: Combination of rs-fMRI and sMRI data to discriminate autism spectrum disorders in young children using deep belief network, Journal of Digital Imaging 31: 895–903; 2018.
3. Christensen DL, Bilder DA, Zahorodny W, et al.: Prevalence and characteristics of autism spectrum disorder among 4-year-old children in the Autism and Developmental Disabilities Monitoring Network. Journal of Developmental & Behavioral Pediatrics 37: 1–8; 2016.
4. Strakowski SM, Fleck DE, Welge J, et al.: fMRI brain activation changes following treatment of a first bipolar manic episode. Bipolar Disorders 18: 490–501; 2016.
5. Courchesne E, Karns C, Davis H, et al.: Unusual brain growth patterns in early life in patients with autistic disorder: An MRI study. Neurology 57: 245–254; 2001.
6. Hazlett HC, Poe M, Gerig G, et al.: Magnetic resonance imaging and head circumference study of brain size in autism: Birth through age 2 years. Archives of General Psychiatry 62: 1366–1376; 2005.
7. Herbert MR, Ziegler DA, Makris N, et al.: Localization of white matter volume increase in autism and developmental language disorder. Annals of Neurology 55: 530–540; 2004.
8. Carper RA, Courchesne E: Localized enlargement of the frontal cortex in early autism. Biological Psychiatry 57: 126–133; 2005.
9. Hardan AY, Muddasani S, Vemulapalli M, et al.: An MRI study of increased cortical thickness in autism. American Journal of Psychiatry 163: 1290–1292; 2006.
10. Ecker C, Ginestet C, Feng Y, et al.: Brain surface anatomy in adults with autism: The relationship between surface area, cortical thickness, and autistic symptoms, JAMA Psychiatry 70: 59–70; 2013.
11. Haar S, Berman S, Behrmann M, Dinstein I: Anatomical abnormalities in autism? Cerebral Cortex 26: 1440–1452; 2014.
12. Zielinski BA, Prigge MB, Nielsen JA, et al.: Longitudinal changes in cortical thickness in autism and typical development. Brain 137: 1799–1812; 2014.
13. Bellani M, Calderoni S, Muratori F, Brambilla P: Brain anatomy of autism spectrum disorders II. Focus on amygdala. Epidemiology and Psychiatric Sciences 22: 309–312; 2013.
14. Waiter GD, Williams JH, Murray AD, et al.: A voxel-based investigation of brain structure in male adolescents with autistic spectrum disorder. Neuroimage 22: 619–625; 2004.
15. Salmond CH, Vargha-Khadem F, Gadian DG, et al.: Heterogeneity in the patterns of neural abnormality in autistic spectrum disorders: Evidence from ERP and MRI. Cortex 43: 686–699; 2007.
16. Hardan AY, Jou RJ, Keshavan MS, et al.: Increased frontal cortical folding in autism: A preliminary MRI study. Psychiatry Research: Neuroimaging 131: 263–268; 2004.
17. Zilles K, Armstrong E, Schleicher A, Kretschmann HJ: The human pattern of gyrification in the cerebral cortex. Anatomy and Embryology 179: 173–179; 1988.
18. Wallace GL, Robustelli B, Dankner N, et al.: Increased gyrification, but comparable

surface area in adolescents with autism spectrum disorders. Brain 136: 1956–1967; 2013.
19. Awate SP, Win L, Yushkevich P, et al. 3D cerebral cortical morphometry in autism: Increased folding in children and adolescents in frontal, parietal, and temporal lobes. In: International Conference on Medical Image Computing and Computer-Assisted Intervention. New York: Springer; 2008. p. 559–567.
20. Katuwal GJ, Cahill ND, Baum SA, Michael AM: The predictive power of structural MRI in autism diagnosis. Annual Conference of the Engineering in Medicine and Biology Society 37: 4270–4273; 2015.
21. Nordahl CW, Dierker D, Mostafavi I, et al.: Cortical folding abnormalities in autism revealed by surface-based morphometry. Journal of Neuroscience 27: 11725–11735; 2007.
22. Dierker DL, Feczko E, Pruett JR Jr, et al.: Analysis of cortical shape in children with simplex autism. Cerebral Cortex 25: 1042–1051; 2013.
23. Ecker C, Andrews D, Dell'Acqua F, et al.: Relationship between cortical gyrification, white matter connectivity, and autism spectrum disorder. Cerebral Cortex 26: 3297–3309; 2016.
24. Cherkassky VL, Kana RK, Keller TA, Just MA: Functional connectivity in a baseline resting-state network in autism. Neuroreport 17: 1687–1690; 2006.
25. Just MA, Cherkassky VL, Keller TA, Minshew NJ: Cortical activation and synchronization during sentence comprehension in high-functioning autism: Evidence of underconnectivity. Brain 127: 1811–1821; 2004.
26. Damarla SR, Keller TA, Kana RK, et al.: Cortical underconnectivity coupled with preserved visuospatial cognition in autism: Evidence from an fMRI study of an embedded figures task. Autism Research 3: 273–279; 2010.
27. Weng SJ, Carrasco M, Swartz JR, et al.: Neural activation to emotional faces in adolescents with autism spectrum disorders. Journal of Child Psychology and Psychiatry 52: 296–305; 2011.
28. Zeeland SV, Ashley A, Dapretto M, et al.: Reward processing in autism. Autism Research 3: 53–67; 2010.
29. Dekhil O, Ismail M, Shalaby A, et al.: A novel CAD system for autism diagnosis using structural and functional MRI. IEEE International Symposium on Biomedical Imaging 14: 995–998; 2017.
30. Dichter GS, Richey JA, Rittenberg AM, et al.: Reward circuitry function in autism during face anticipation and outcomes. Journal of Autism and Developmental Disorders 42: 147–160; 2012.
31. Deshpande G, Libero L, Sreenivasan KR, et al.: Identification of neural connectivity signatures of autism using machine learning. Frontiers in Human Neuroscience 7: 670; 2013.
32. Itahashi T, Yamada T, Watanabe H, et al.: Altered network topologies and hub organization in adults with autism: A resting-state fMRI study. PLoS One 9: e94115; 2014.
33. Rausch A, Zhang W, Haak KV, et al.: Altered functional connectivity of the amygdaloid input nuclei in adolescents and young adults with autism spectrum disorder: A resting

state fMRI study. Molecular Autism 7: 13; 2016.
34. Tyszka JM, Kennedy DP, Paul LK, Adolphs R: Largely typical patterns of resting-state functional connectivity in high-functioning adults with autism. Cerebral Cortex 24: 1894–1905; 2013.
35. Plitt M, Barnes KA, Martin A: Functional connectivity classification of autism identifies highly predictive brain features but falls short of biomarker standards. NeuroImage: Clinical 7: 359–366; 2015.
36. Hahamy A, Behrmann M, Malach R: The idiosyncratic brain: Distortion of spontaneous connectivity patterns in autism spectrum disorder. Nature Neuroscience 18: 302; 2015.
37. Supekar K, Uddin LQ, Khouzam A, et al. Brain hyperconnectivity in children with autism and its links to social deficits. Cell Reports 5: 738–747; 2013.
38. Di Martino A, Yan CG, Li Q, et al.: The Autism Brain Imaging Data Exchange: Towards a large-scale evaluation of the intrinsic brain architecture in autism. Molecular Psychiatry 19: 659; 2014.
39. Suk HI, Lee SW, Shen D, Alzheimer's Disease Neuroimaging Initiative: Latent feature representation with stacked auto-encoder for AD/MCI diagnosis. Brain Structure and Function 220: 841–859; 2015.
40. Kim J, Calhoun VD, Shim E, Lee JH: Deep neural network with weight sparsity control and pre-training extracts hierarchical features and enhances classification performance: Evidence from whole-brain resting-state functional connectivity patterns of schizophrenia. Neuroimage 124: 127–146; 2016.
41. Heinsfeld AS, Franco AR, Craddock RC, et al.: Identification of autism spectrum disorder using deep learning and the ABIDE dataset. NeuroImage: Clinical 17: 16–23; 2018.
42. Sled JG, Zijdenbos AP, Evans AC: A nonparametric method for automatic correction of intensity nonuniformity in MRI data. IEEE Transactions on Medical Imaging 17: 87–97; 1998.
43. Ségonne F, Dale AM, Busa E, et al.: A hybrid approach to the skull stripping problem in MRI. Neuroimage 22: 1060–1075; 2004.
44. Fischl B, Salat DH, Van Der Kouwe AJ, et al.: Sequence-independent segmentation of magnetic resonance images. Neuroimage 23: S69–S84; 2004.
45. Fischl B, Salat DH, Busa E, et al.: Whole brain segmentation: Automated labeling of neuroanatomical structures in the human brain. Neuron 33: 341–355; 2002.
46. Fischl B, Liu A, Dale AM: Automated manifold surgery: Constructing geometrically accurate and topologically correct models of the human cerebral cortex. IEEE Transactions on Medical Imaging 20: 70–80; 2001.
47. Ségonne F, Pacheco J, Fischl B: Geometrically accurate topology-correction of cortical surfaces using nonseparating loops. IEEE Transactions on Medical Imaging 26: 518–529; 2007.
48. Fischl B, Sereno MI, Dale AM: Cortical surface-based analysis: II: inflation, flattening, and a surface-based coordinate system. Neuroimage 9: 195–207; 1999.
49. Fischl B, Sereno MI, Tootell RB, Dale AM: High-resolution intersubject averaging and a coordinate system for the cortical surface. Human Brain Mapping 8: 272–284; 1999.
50. Desikan RS, Ségonne F, Fischl B, et al.: An automated labeling system for subdividing the human cerebral cortex on mri scans into gyral based regions of interest. Neuroimage 31:

968–980; 2006.
51. Van Den Heuvel MP, Pol HEH: Exploring the brain network: A review on resting-state fMRI functional connectivity. European Neuropsychopharmacology 20: 519–534; 2010.
52. Casanova EL, Casanova MF. Defining Autism. London: Jessica Kingsley; 2018.
53. Kanner L: Autistic disturbances of affective contact. Nervous Child 2: 217–250; 1943.
54. Estes A, Munson J, Rogers SJ, et al.: Long-term outcomes of early intervention in 6-year-old children with autism spectrum disorder. Journal of the American Academy of Child & Adolescent Psychiatry 54: 580–587; 2015.
55. Dekhil O, Hajjdiab H, Ayinde B, et al.: Using resting state functional MRI to build a personalized autism diagnosis system PLoS One 13: e0206351; 2018.
56. Dekhil O, Ali M, Shalaby A, et al. Identifying personalized autism related impairments using resting functional MRI and ADOS reports. In: International Conference on Medical Image Computing and Computer-Assisted Intervention. New York: Springer; 2018. p. 240–248.
57. Piven J, Elison JT, Zylka MJ: Toward a conceptual framework for early brain and behavior development in autism. Molecular Psychiatry 22: 1385; 2017.
58. Casanova MF, El-Baz A, Mott M, et al.: Reduced gyral window and corpus callosum size in autism: Possible macroscopic correlates of a minicolumnopathy. Journal of Autism and Developmental Disorders 39: 751–764; 2009.
59. Hofman MA. Brain evolution in hominids: Are we at the end of the road? In: Falk D, Gibson K, editors. Evolutionary anatomy of the primate cerebral cortex. Cambridge: Cambridge University Press; 2001. p. 113–127.

Tables

Table 1: The eight extracted features and their description for the sMRI experiment

Feature	Description
SA	Surface area per DK atlas area
V	Volume per DK atlas area
T	Average thickness per DK atlas area
Tstd	Standard deviation of thickness in DK atlas area
MCI	Mean of the 2 principal curvature per DK atlas area
K	Mean of Gaussian curvature per DK atlas area
ICI	Mean of intrinsic curvature per DK atlas area
FI	Average of folding index index per DK atlas area

Table 2: The cohort summary statistics of each site in the used dataset

UCLA				
		ASD		
males	48	females	6	
	min.	max.	mean	s.d.
Age	8.36	17.94	13.0	2.4
VIQ	67.0	132.0	101. 6	14.0
FSIQ	67.0	128.0	98.2	18.7
PIQ	73.0	132.0	99.8	13.7
		TD		
males	38	females	6	
	min.	max.	mean	s.d.
Age	9.21	17.79	13.0	1.9
VIQ	86.0	127.0	107.1	11.4
FSIQ	86.0	128.0	106.4	11.0
PIQ	76.0	129.0	104.3	11.6
NYU				
		ASD		
males	65	females	10	
	min.	max.	mean	s.d.
Age	7.13	39.1	14.7	7.0
VIQ	73.0	139.0	104.9	15.8
FSIQ	73.0	148.0	107.1	16.2
PIQ	72.0	149.0	108.3	17.1
		TD		
males	74	females	26	
	min.	max.	mean	s.d.
Age	6.47	31.78	15.7	6.1
VIQ	80.0	143.0	112.8	12.6
FSIQ	80.0	142.0	113.0	13.3
PIQ	67.0	137.0	110.2	13.9
Leuven				
		ASD		
males	26	females	3	
	min.	max.	mean	s.d.
Age	12.1	32.0	17.8	4.9
VIQ	50.0	128.0	99.1	19.7
FSIQ	50.0	128.0	100.2	31.6
PIQ	74.0	149.0	103.7	16.5
		TD		
males	29	females	5	

	min.	max.	mean	s.d.
Age	12.2	29.0	18.2	5.0
VIQ	86.0	136.0	116.4	10.7
FSIQ	86.0	146.0	107.6	30.3
PIQ	84.0	155.0	108.0	12.9
Caltech				
		ASD		
males	15	females	4	
	min.	max.	mean	s.d.
Age	17.5	55.4	27.4	10.0
VIQ	80.0	135.0	107.7	15.0
FSIQ	80.0	133.0	108.2	12.2
PIQ	84.0	128.0	107.4	11.4
		TD		
males	14	females	4	
	min.	max.	mean	s.d.
Age	17.0	56.2	28.0	10.6
VIQ	85.0	135.0	114.5	12.4
FSIQ	85.0	134.0	114.8	9.3
PIQ	96.0	129.0	111.8	9.2
MAXMUN				
		ASD		
males	21	females	3	
	min.	max.	mean	s.d.
Age	7.0	58.0	26.1	14.6
VIQ	0	0	0.0	0.0
FSIQ	0	133.0	109.9	14.2
PIQ	99.0	122.0	111.5	9.4
		TD		
males	27	females	1	
	min.	max.	mean	s.d.
Age	7.0	46.0	24.6	8.6
VIQ	0	0	0.0	0.0
FSIQ	0	129.0	111.8	9.1
PIQ	83.0	126.0	110.9	13.4
OLIN				
		ASD		
males	16	females	3	
	min.	max.	mean	s.d.
Age	11.0	24.0	16.5	3.3
VIQ	0	0	0.0	0.0
FSIQ	0	135.0	112.6	17.8

PIQ	0	0	0.0	0.0
		TD		
males	13	females	2	
	min.	max.	mean	s.d.
Age	10.0	23.0	16.7	3.5
VIQ	0	0	0.0	0.0
FSIQ	0	135.0	113.9	16.0
PIQ	0	0	0.0	0.0
KKI				
		ASD		
males	16	females	4	
	min.	max.	mean	s.d.
Age	8.09	12.54	10.0	1.4
VIQ	0	0	0.0	0.0
FSIQ	0	131.0	93.45	27.3
PIQ	0	0	0.0	0.0
		TD		
males	20	females	8	
	min.	max.	mean	s.d.
Age	8.07	12.77	10.0	1.1
VIQ	0	0	0.0	0.0
FSIQ	0	125.0	112.1	9.2
PIQ	0	0	0.0	0.0
OHSU				
		ASD		
males	12	females	0	
	min.	max.	mean	s.d.
Age	8.0	15.23	11.4	2.1
VIQ	0	0	0.0	0.0
FSIQ	0	132.0	106.0	21.0
PIQ	0	0	0.0	0.0
		TD		
males	14	females	0	
	min.	max.	mean	s.d.
Age	8.2	11.99	10.1	1.1
VIQ	0	0	0.0	0.0
FSIQ	0	132.0	115.0	10.7
PIQ	0	0	0.0	0.0
Pitt				
		ASD		
males	25	females	4	
	min.	max.	mean	s.d.

Age	9.33	35.2	19.0	7.2
VIQ	81.0	132.0	107.0	13.5
FSIQ	81.0	131.0	110.2	14.3
PIQ	83.0	128.0	110.8	13.9
		TD		
males	23	females	4	
	min.	max.	mean	s.d.
Age	9.44	33.24	18.9	6.5
VIQ	88.0	132.0	107.7	10.8
FSIQ	88.0	130.0	110.1	9.2
PIQ	90.0	123.0	109.6	8.8
SBL				
		ASD		
males	15	females	0	
	min.	max.	mean	s.d.
Age	22.0	64.0	35.0	10.1
VIQ	93.0	133.0	110.4	11.9
FSIQ	93.0	125.0	109.2	12.2
PIQ	84.0	135.0	114.2	11.6
		TD		
males	15	females	0	
	min.	max.	mean	s.d.
Age	20.0	42.0	33.7	6.4
VIQ	0	0	0.0	0.0
FSIQ	0	0	0.0	0.0
PIQ	0	0	0.0	0.0
SDSU				
		ASD		
males	13	females	1	
	min.	max.	mean	s.d.
Age	12.13	17.15	14.7	1.7
VIQ	83.0	147.0	110.1	17.7
FSIQ	83.0	141.0	103.3	33.5
PIQ	81.0	140.0	109.7	15.8
		TD		
males	16	females	6	
	min.	max.	mean	s.d.
Age	8.67	16.88	14.2	1.9
VIQ	87.0	126.0	106.7	10.2
FSIQ	87.0	126.0	108.1	10.3
PIQ	86.0	129.0	107.8	11.9
Stanford				

		ASD		
males	15	females	4	
	min.	max.	mean	s.d.
Age	7.5	12.9	10.0	1.6
VIQ	72.0	149.0	108.3	19.9
FSIQ	72.0	141.0	110.7	15.7
PIQ	89.0	129.0	110.6	12.1
		TD		
males	16	females	4	
	min.	max.	mean	s.d.
Age	7.8	12.4	10.0	1.6
VIQ	67.0	144.0	111.2	19.2
FSIQ	67.0	136.0	112.1	15.0
PIQ	81.0	145.0	110.6	15.2
Trinty				
		ASD		
males	22	females	0	
	min.	max.	mean	s.d.
Age	12.0	23.08	16.8	3.1
VIQ	85.0	135.0	107.9	14.0
FSIQ	85.0	135.0	105.3	29.2
PIQ	63.0	131.0	107.6	15.3
		TD		
males	25	females	0	
	min.	max.	mean	s.d.
Age	12.04	25.66	17.1	3.7
VIQ	81.0	137.0	109.6	13.4
FSIQ	81.0	133.0	110.9	12.0
PIQ	84.0	132.0	110.3	10.7
UM				
		ASD		
males	57	females	9	
	min.	max.	mean	s.d.
Age	8.5	18.6	13.2	2.4
VIQ	75.0	180.0	108.7	19.9
FSIQ	75.0	147.5	105.5	17.1
PIQ	59.0	148.0	102.6	19.9
		TD		
males	56	females	18	
	min.	max.	mean	s.d.
Age	8.2	28.8	14.8	3.6
VIQ	86.0	147.0	113.6	12.7

FSIQ	86.0	129.0	108.2	9.7
PIQ	72.0	127.0	103.1	12.1
USM				
		ASD		
males	46	females	0	
	min.	max.	mean	s.d.
Age	11.4	50.2	23.5	8.2
VIQ	55.0	130.0	95.0	19.1
FSIQ	55.0	132.0	97.4	21.9
PIQ	72.0	133.0	104.7	16.5
		TD		
males	25	females	0	
	min.	max.	mean	s.d.
Age	8.8	39.4	21.3	8.2
VIQ	87.0	140.0	113.6	15.7
FSIQ	87.0	144.0	115.4	14.8
PIQ	90.0	138.0	112.8	13.9
Yale				
		ASD		
males	20	females	8	
	min.	max.	mean	s.d.
Age	7.0	17.75	12.7	3.0
VIQ	42.0	143.0	96.5	22.7
FSIQ	42.0	141.0	94.6	21.2
PIQ	37.0	126.0	92.3	18.9
		TD		
males	20	females	8	
	min.	max.	mean	s.d.
Age	7.66	17.83	12.7	2.7
VIQ	73.0	140.0	106.8	15.7
FSIQ	73.0	140.0	105.0	17.1
PIQ	76.0	139.0	101.3	16.2

Table 3: The obtained accuracy, sensitivity, specificity and area under ROC curve of the sMRI experiment and the corresponding number of the concatenated feature.

	sMRI RESULTS				
site	Accuracy	Sensitivity	Specificity	AUC	number of features
UCLA	0.898	0.972	0.855	0.950	72
NYU	0.749	0.733	0.782	0.787	53
Leuven	0.921	0.914	0.929	0.935	14
CMU	1	1	1	1	13
Caltech	0.946	0.900	1	0.980	59
MaxMun	0.962	0.964	0.958	0.969	23
Olin	0.912	0.875	0.944	0.958	13
KKI	0.9167	0.900	0.944	0.938	30
OHSU	1	1	1	1	5
Pitt	0.946	0.962	0.933	0.963	35
SBL	1	1	1	1	10
SDSU	0.917	0.913	0.923	0.932	25
Stanford	0.897	0.944	0.857	0.942	23
Trinity	0.915	0.920	0.909	0.943	76
UM	0.814	0.800	0.833	0.843	27
USM	0.901	0.950	0.882	0.922	21
Yale	0.946	0.931	0.963	0.987	75

Table 4: The obtained accuracy, sensitivity, specificity and area under ROC curve of the fMRI experiment and the corresponding number of the concatenated feature

	fMRI RESULTS				
Source	Accuracy	Sensitivity	Specificity	AUC	number of features
UCLA	0.836	0.804	0.865	0.855	99
NYU	0.794	0.796	0.790	0.817	96
Leuven	0.952	0.942	0.964	0.993	81
CMU	0.925	0.923	0.928	0.972	19
Caltech	0.972	0.947	1	0.985	83
MaxMun	0.865	0.8	1	0.904	17
Olin	1	1	1	1	20
KKI	0.958	0.933	1	0.978	45
OHSU	0.946	0.813	0.900	0.863	16
Pitt	0.892	0.920	0.870	0.919	94
SBL	0.966	0.937	1	0.991	43
SDSU	0.916	0.880	1	0.89	22
Stanford	0.974	1	0.950	1	50
Trinity	0.978	1	0.956	0.994	76
UM	0.785	0.775	0.800	0.860	88
USM	0.887	0.947	0.865	0.916	43
Yale	0.964	0.964	0.964	0.965	65

Figure captions

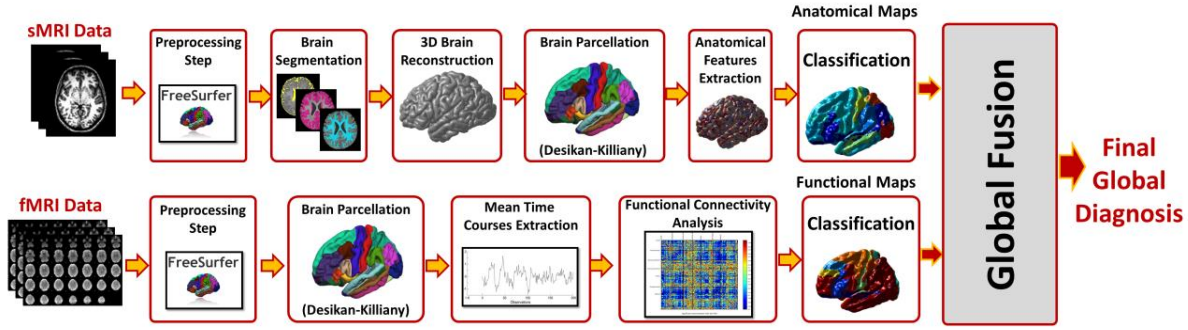

Figure 1: The overall pipeline of the proposed approach, for each modality preprocessing and analysis is applied to calculate the feature matrix. The features of the modality are fed to a local classifier, modality fusion decision is then calculated and finally overall diagnosis decision is reported using both sMRI and fMRI decisions

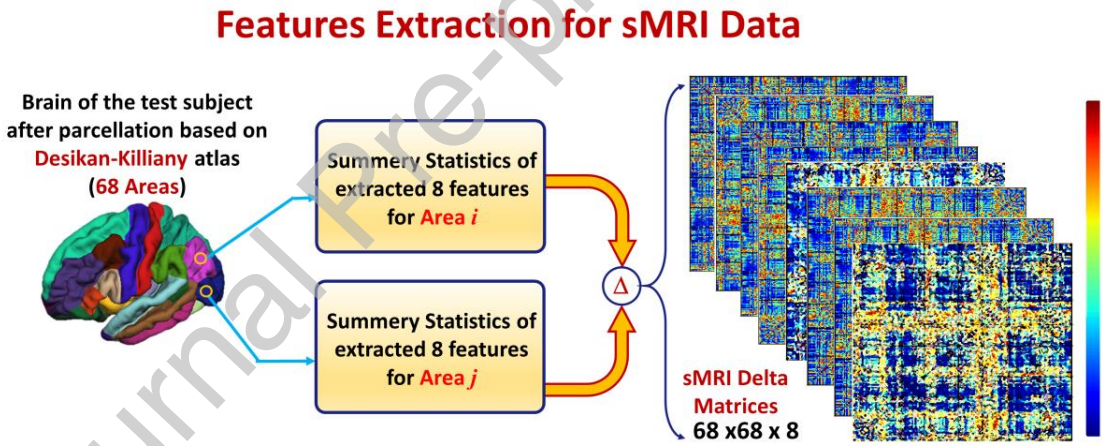

Figure 2: Eight features are extracted from the parcellated volume, summary statistics are calculated for each feature at each DK atlas area. Then, Delta matrix for each subject is calculated by subtracting the feature values between each couple of areas. The output feature matrix is 68x68x8.

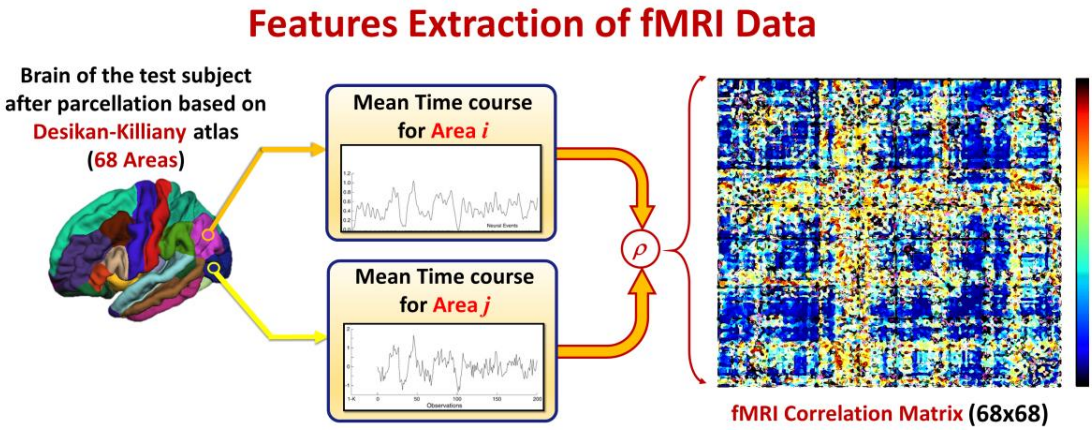

Figure 3: For each couple of areas the correlation coefficient between the time courses is calculated to form 1 68x86 feature matrix

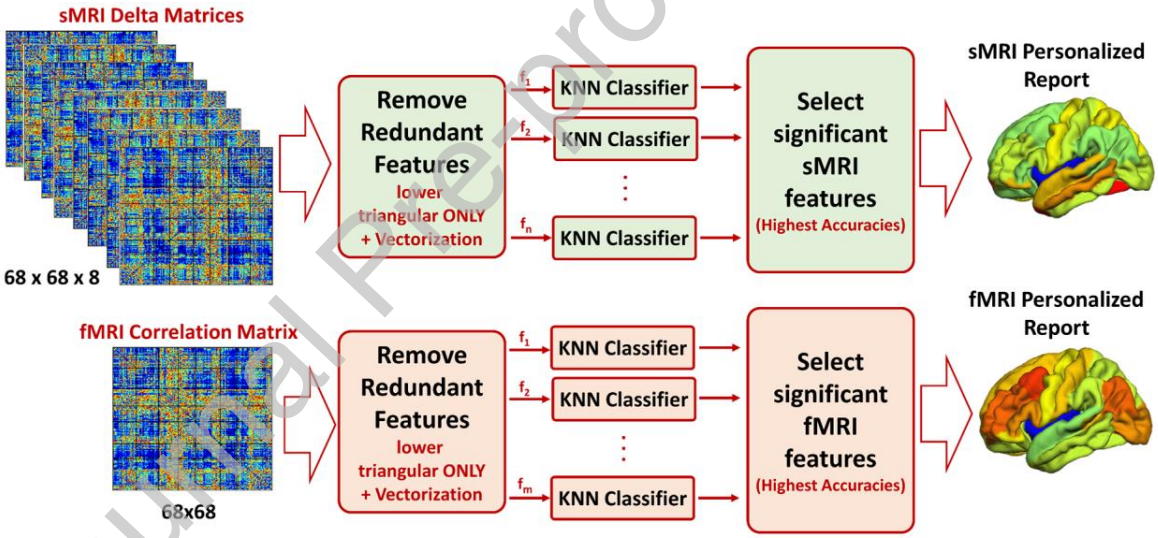

Figure 4: The 2 stages classification approach used. In the first stage, a local classification per each feature in sMRI and fMRI feature matrices is used. The output accuracies of the first stage are used to create a sorted feature vectors. An incremental approach is used to determine the optimal length of the sMRI and fMRI feature vectors. These 2 vectors are finally concatenated for the global classification

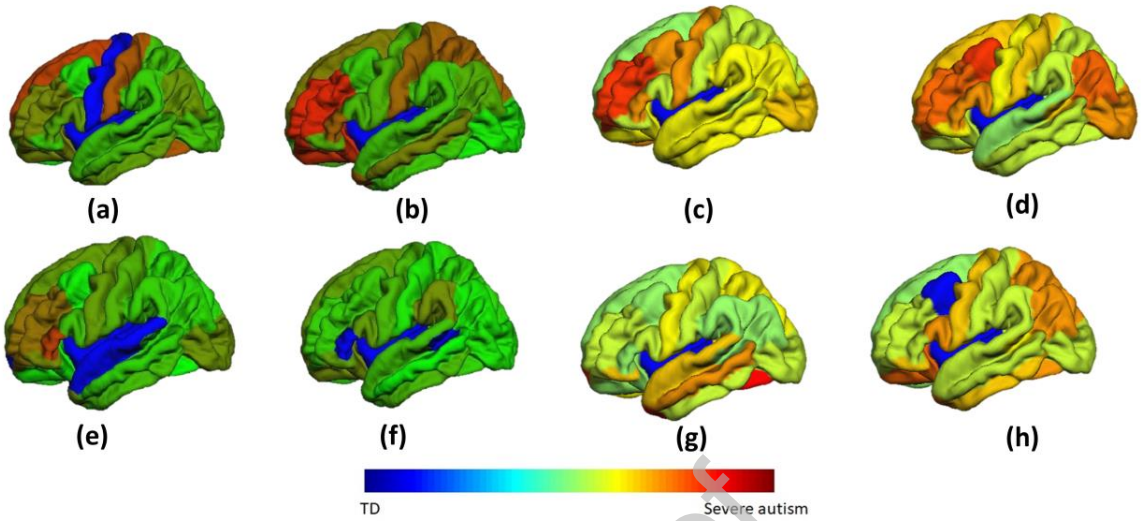

Figure 5: A sample of the generated personalized maps for 8 subjects: (a,b) are the personalized maps of 2 ASD subjects obtained from sMRI local classification, (c,d) are the personalized maps of 2 ASD subjects obtained from fMRI local classification, (e,f) are the personalized maps of 2 TD subjects obtained from sMRI local classification, and (g,h) are the personalized maps of 2 TD subjects obtained from fMRI local classification.